Journal of Biomedical Optics

SPIEDigitalLibrary.org/jbo

Evaluation of optical reflectance techniques for imaging of alveolar structure

Carolin I. Unglert
Eman Namati
William C. Warger, II
Linbo Liu
Hongki Yoo
DongKyun Kang
Brett E. Bouma
Guillermo J. Tearney

SPIE

Evaluation of optical reflectance techniques for imaging of alveolar structure

Carolin I. Unglert,[a,b] Eman Namati,[a] William C. Warger II,[a] Linbo Liu,[a] Hongki Yoo,[a] DongKyun Kang,[a] Brett E. Bouma,[a,c] and Guillermo J. Tearney[a,c,d]
[a]Wellman Center for Photomedicine, Harvard Medical School and Massachusetts General Hospital, 40 Parkman Street, RSL 160, Boston, Massachusetts 02114
[b]Air Liquide Centre de Recherche Claude-Delorme, Medical Gases Group, 1 Chemin de la Porte des Loges, Les-Loges-en-Josas, France
[c]Harvard-MIT Division of Health Sciences and Technology, 77 Massachusetts Avenue, Cambridge, Massachusetts 02139
[d]Massachusetts General Hospital, Department of Pathology, Boston, Massachusetts 02114

Abstract. Three-dimensional (3-D) visualization of the fine structures within the lung parenchyma could advance our understanding of alveolar physiology and pathophysiology. Current knowledge has been primarily based on histology, but it is a destructive two-dimensional (2-D) technique that is limited by tissue processing artifacts. Micro-CT provides high-resolution three-dimensional (3-D) imaging within a limited sample size, but is not applicable to intact lungs from larger animals or humans. Optical reflectance techniques offer the promise to visualize alveolar regions of the large animal or human lung with sub-cellular resolution in three dimensions. Here, we present the capabilities of three optical reflectance techniques, namely optical frequency domain imaging, spectrally encoded confocal microscopy, and full field optical coherence microscopy, to visualize both gross architecture as well as cellular detail in fixed, phosphate buffered saline-immersed rat lung tissue. Images from all techniques were correlated to each other and then to corresponding histology. Spatial and temporal resolution, imaging depth, and suitability for *in vivo* probe development were compared to highlight the merits and limitations of each technology for studying respiratory physiology at the alveolar level.
[DOI: 10.1117/1.JBO.17.7.071303]

Keywords: backscattering; biomedical optics; coherent optics; confocal optics; medical imaging; optical coherence tomography; alveolar imaging.

Paper 11627SS received Oct. 26, 2011; revised manuscript received Dec. 21, 2011; accepted for publication Dec. 29, 2011; published online Jun. 11, 2012.

1 Introduction

The visualization of pulmonary alveolar structure is crucial to advance our understanding of the functional unit of the lung and its pathologies. Important knowledge has been derived from histological sections that provide insights into the architecture of the peripheral lung at the subcellular level. Histologic stains provide contrast for collagen and elastin within the alveolar wall, type I and type II pneumocytes, and capillaries to differentiate healthy and diseased alveolar tissue. While histology continues to be the gold standard for studying alveolar structure, it is a two-dimensional (2-D), destructive technique. Three-dimensional (3-D) data can only be estimated by stereologic methods[1] or be obtained through careful registration of serial sections.[2] Moreover, once the tissue has been cut to obtain histologic sections, it is no longer available for subsequent analysis with alternative techniques or stains. In addition, mechanical distortion caused by embedding and sectioning the tissue can lead to incorrect morphological analysis.[1]

Micro-CT provides non-destructive, 3-D assessment of alveolar structures[3] with isotropic pixel sizes on the order of 9 μm for sample thicknesses of 8 mm and much higher resolutions can be reached for smaller samples (400 nm for 200 μm thick samples[4]). However, the resolution decreases with increasing sample thickness, such that alveolar structures cannot be sufficiently visualized within whole animal models. Further, the potential of micro-CT for *in vivo* quantification of mammalian alveoli is limited due to low soft-tissue contrast, relatively slow scanning speed, and exposure to ionizing radiation.[5]

An ideal imaging modality for the assessment of alveolar structure would not be subject to processing artifacts and provide 3-D data with sufficient spatial resolution to clearly delineate alveolar morphology ($\leq$10 μm) or cellular detail ($\leq$5 μm) across species. Lastly, a technology that is non-toxic with temporal resolution less than the breathing rate could allow *in vivo* assessment of alveolar dynamics to provide additional insights into tissue mechanics as well as pathophysiologic changes occurring over time within the same animal.

Optical reflectance techniques, including confocal microscopy and Fourier-domain optical coherence tomography (OCT) have recently been used for 3-D imaging of alveolar structure with spatial resolutions on the order of 1 to 10 μm.[6,7] As these technologies utilize backscattered light, resolution is independent of the sample size and can be obtained within intact lungs *in situ* and across all species. The imaging depth, however, is limited to only a few layers of alveoli. Optical reflectance techniques have potential for *in vivo* assessment because they can provide images at speeds that are greater than video rate, thereby mitigating motion artifacts, and do not require contrast agents or ionizing radiation.

The goal of this study is to compare the capabilities of three advanced optical reflectance techniques for visualizing the

Address all correspondence to: Carolin I. Unglert, Wellman Center for Photomedicine, Harvard Medical School and Massachusetts General Hospital, 40 Parkman Street, RSL 160, Boston, Massachusetts 02114. Tel.: +617 724 1359; Fax: 617 726 4103; E-mail: cunglert@mgh.harvard.edu

0091-3286/2012/$25.00

structures of the peripheral lung, evaluate their potential to complement existing tools, such as histology and micro-CT, and assess their potential for *in vivo* use. We have investigated optical frequency domain imaging (OFDI), spectrally encoded confocal microscopy (SECM), and full field optical coherence microscopy (FFOCM), expecting to find that these modalities supply complimentary information due to their range of contrast, spatial, and temporal resolutions. OFDI, which can also be referred to as swept-source Fourier-domain OCT, is a high-speed, 10-μm resolution, interferometric cross-sectional imaging technique[8,9] that provides structural information over larger fields of view. SECM is a high-speed, high resolution (1 μm lateral, 2.3 μm axial resolution) confocal microscopy technique[10] that allows comprehensive evaluation of cellular details in larger tissue samples. FFOCM, an additional interferometric technique similar to OCT, is a high resolution (1-μm isotropic) *en-face* imaging modality, based on wide-field interferometry,[11] suitable for the evaluation of cellular details over a small field of view. Fixed rat lung slices immersed within phosphate buffered saline (PBS) were imaged to compare the three technologies over the same field of view at the same inflation. The rat lung parenchyma is a good representative of mammalian lung parenchyma tissue and is a popular animal model for pulmonary diseases.[12–15]

2 Materials and Methods

2.1 *Sample Preparation*

All animal experiments were approved and carried out in accordance with the regulations set forth by the Massachusetts General Hospital Subcommittee on Research Animal Care. Three adult Sprague-Dawley rats (approximately 350 g) were weighed and anesthetized with an intramuscular injection of Ketamine-Xylazine. Once a surgical plane of anesthesia was reached, the abdominal aorta was transected to exsanguate the animals. The trachea was then exposed and catheterized with an 18 G catheter. The lungs were instillation fixed *in situ* at 20 cm H_2O pressure through a gravity feed system using a modified Heitzman solution consisting of 10% formaldehyde solution (Fisher Scientific), 10% ethanol (Fisher Scientific), 25% polyethylene glycol 400 (Post Apple Scientific), and 55% laboratory distilled water.[16] After 30 min, the lungs were carefully excised and then immersed within the Heitzman solution while connected to the feed system at the same inflation pressure for a minimum of 48 h. The lungs were then disconnected from the fixation apparatus and air-dried for a minimum of 2 days in a 60°C drying oven while pressurized with air at 20 cm H_2O. Finally, the dry inflated lungs were cut into cylindrical sections, approximately 3 mm in diameter and 1 to 2 mm thick, immersed in PBS and degassed for imaging. After 3-D images were obtained with all three imaging modalities on the same sample, each was placed in formalin and the entire sample was processed for paraffin-embedded histopathology by using standard methods. Five micrometer thick Hematoxylin and eosin (H&E) histopathology slices were obtained, and slides were digitized by using a full-slide scanner (ScanScope CS, Aperio Technologies, Inc, Vista, Calif).

2.2 *Imaging Techniques*

Three different optical reflectance-imaging technologies were used to obtain the same approximate field of view within each sample. First, OFDI and SECM images were acquired with a 200 μm thick cover glass between the sample and the focusing optics, and then the cover glass was removed and the sample was imaged with FFOCM. In this section, we describe the basic functionality and system components of each technique. The characteristics of each imaging modality are summarized in Table 1.

Table 1 OFDI, SECM, and FFOCM system parameters used to image PBS-immersed rat lung tissue.

Parameter	OFDI	SECM	FFOCM
Image orientation	Cross-section	*En-face*	*En-face*
NA	0.08	*1.2*	*0.45*
Transverse resolution (μm)	12	1.3	1
Axial resolution (μm)	*7*	2.4	1
Acquired volumes (mm × mm × mm)	2 × 2 × 5[a]	2 × 2 × 0.2	0.25 × 0.25 × 0.25
Acquisition time (min)	0.07	30	60

[a]The ranging depth in PBS is 5 mm.

2.2.1 *OFDI*

OFDI is an interferometric technique based on optical frequency-domain reflectometry.[8,17–19] With OFDI, a wavelength swept source with a broad tuning range, illuminates the sample, and the backscattered light recombines with a reference arm that is reflected from a stationary mirror. The resultant interferogram from one complete sweep of the laser bandwidth is then Fourier transformed to provide the reflectivity as a function of depth (A-line) within the tissue. A galvanometric scanner scans the illumination beam in a raster pattern on the tissue surface to reconstruct a 3-D volume. The axial resolution is dependent on the bandwidth of the laser[8] and is decoupled from the lateral resolution,[20] which is dependent on the numerical aperture (NA) of the imaging lens (0.08 NA, 30 mm focal length, Thorlabs). Our OFDI system has a 62.5 kHz wavelength-swept source, with a 110 nm bandwidth centered at 1310 nm, providing fast ($>100\,\mathrm{cross-sectional\,frames/s}$) imaging with high isotropic resolution (10 μm) over large depths in tissue (1 to 2 mm). The technique has been fully integrated into small imaging probes, making it particularly well suited for *in vivo* imaging of tissue architecture.[21] In this study, a bench top raster scanning probe was used to obtain fields of view of 2×2 mm (512×512 pixels) over a ranging depth of 5 mm (in water) in 4 s.

2.2.2 *SECM*

SECM[10,22] is a reflectance confocal microscopy technique that uses broadband light to illuminate a diffraction grating-lens pair. This configuration focuses a line of spectrally dispersed light into the sample, where each point along the line illuminates the sample with a different wavelength. Light reflected from the sample returns back through the grating-lens pair and then through an aperture, which provides optical sectioning.

The simultaneous detection of the spectrally-encoded line eliminates the need for a mechanical scanning mechanism along the spectrally encoded dimension, and a single scanner sweeps the line to provide a 2-D image. Large fields of view are obtained by mosaicing the scan pattern with a stage scanner. The system used in this study[23] uses a wavelength-swept source with a 1320 nm center wavelength, 70 nm bandwidth, and a 5 kHz repetition rate. The combination of a 1100 lines/mm transmission diffraction grating and a 3 mm focal length objective lens (Olympus 60×, 1.2 NA in water, 350 μm working distance) provides a 0.12 mm spectrally encoded line. Translation stages in the transverse and axial directions scan the sample to image a $2 \times 2 \times 0.2$ mm volume ($4000 \times 4000 \times 40$ pixels), in approximately 30 min. SECM was integrated in this study because it can provide high transverse resolution (1.3 μm transverse and 2.4 μm axial) over a large field of view.[10,24]

2.2.3 *FFOCM*

FFOCM[11] uses a spatially incoherent light source to illuminate the reference and sample arms of a Linnik interferometer. *En-face* images are then reconstructed by processing the resultant interference patterns from the backscattered light at discrete reference arm lengths with a phase-shifting algorithm. The FFOCM system used in this study,[25] uses a broadband Xenon arc lamp (450 to 750 nm) that illuminates a reference arm mirror and sample through two identical water-immersion objective lenses (Olympus 20×, 0.45 NA in water, working distance 3 mm). The resultant interference pattern is detected by a high-speed CMOS area scan camera (peak response at 600 nm). Images are acquired as the reference arm mirror moves and 2-D *en-face* images at one depth location are reconstructed by demodulating the image interference pattern.[11] Images from different axial locations are obtained by translating the sample arm objective so that the focal location changes within the tissue. Volumes of $0.25 \times 0.25 \times 0.25$ mm ($512 \times 512 \times 1000$ pixels) were obtained within approximately 60 min. FFOCM was integrated in this study to visualize sub-cellular structures in the peripheral lung with isotropic 1 μm resolution.

3 Results and Discussion

3.1 *OFDI*

Figure 1(a) shows a typical cross-sectional OFDI image of a rat lung slice, where the alveoli appear as dark gaps within the highly scattering tissue under the cover glass. Figure 1(b) shows the orthogonal *en-face* image from the sample with the corresponding H&E histology section shown in Fig. 1(c). Single alveoli can be easily distinguished within the OFDI images up to a depth of approximately 500 μm and the presence of the fixed blood vessels (marked with a V) does not appear to decrease the overall imaging depth significantly. The alveolar wall thickness appears overestimated (25 ± 6 μm full width at half maximum (FWHM), mean $\pm$ standard deviation, $n = 31$) compared with the generally accepted wall thickness of a rat alveolus (7 to 10 μm).

3.2 *SECM*

Figure 2(a) shows a wide-field *en-face* SECM image with the corresponding H&E histology in Fig. 2(b) for a rat lung slice approximately 70 μm in depth from the top surface of the slice. The wide-field SECM image demonstrates the ability to visualize relatively large fields of view with cellular-level detail. Figure 2(c) to 2(d) shows how a zoomed-in region of a SECM image with corresponding histology to demonstrate how the airway epithelium, vessel endothelium and blood, and aggregations of cell nuclei can be characterized by bright SECM signal. Type II alveolar pneumocytes (arrows) were directly matched between SECM and histology.

The maximum imaging depth was dependent on the structure. Blood filled vessels and the surrounding collagen matrix provide high contrast up to 150 μm into the specimen, but alveolar walls were difficult to identify for imaging depths greater than 100 μm. Thirty randomly chosen alveolar walls were measured with a FWHM thickness of 5.5 ± 6.1 μm (mean$\pm$ standard deviation). It is important to note, that in some histology slides, the structures appear to be distorted or reduced in size, which may have been caused by histologic tissue processing required to obtain the H&E stained slides. Although best

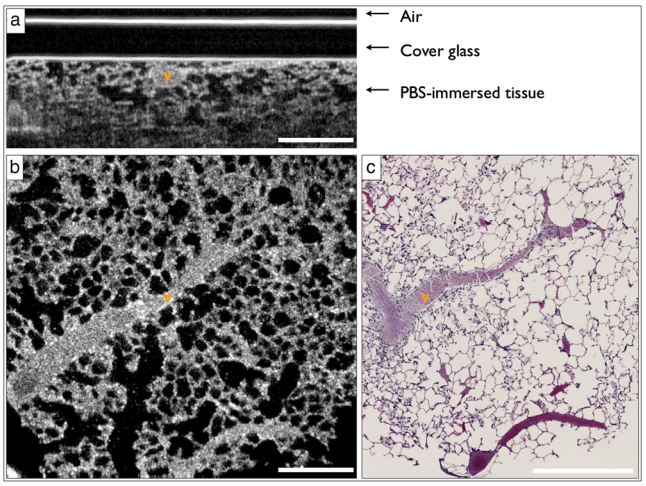

Fig. 1 OFDI and H&E histology images of PBS-immersed fixed rat lung slice. (a) Axial cross-section and (b) *en-face* OFDI images. (c) Corresponding H&E histology sectioned in *en-face* plane. V indicates a vessel within the tissue. Scale bars, 500 μm.

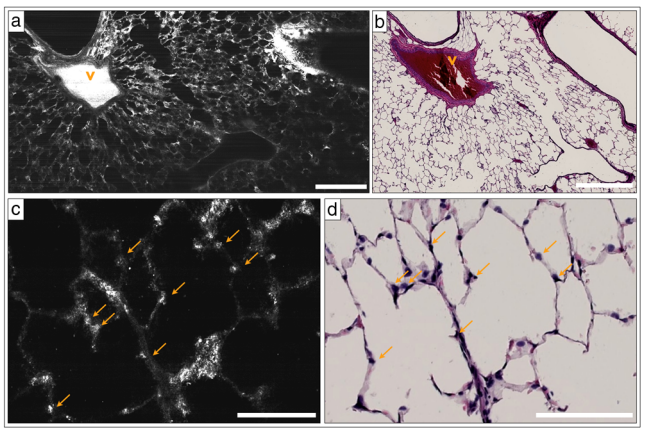

Fig. 2 SECM and H&E histology images of PBS-immersed fixed rat lung slice. (a) *En-face* SECM image 70 μm within tissue and (b) corresponding H&E histology, where V indicates a vessel and scale bar = 500 μm. (c) SECM image in greater detail and (d) corresponding H&E histology, where arrows indicate alveolar type II pneumocytes and scale bar = 100 μm.

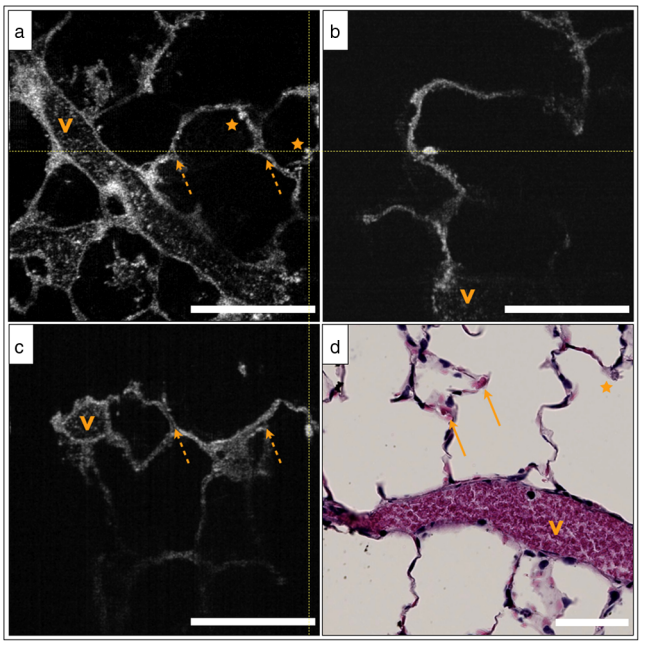

Fig. 3 FFOCM and H&E histology images of PBS-immersed fixed rat lung slice. (a) *En-face*, (b) axial cross-section, and (c) orthogonal axial cross-section images obtained with FFOCM, where dotted lines show the orientation of axial cross-sections intersecting at a three-dimensional type II pneumocyte. (d) Representative H&E histology slide from nearby location sectioned in *en-face* plane. Stars indicate alveolar type II pneumocytes, V indicates a blood vessel containing crenated blood cells, and dotted arrows indicate capillaries in alveolar walls. Scale bars = 100 μm.

efforts were made to ensure that the SECM and H&E section were parallel, there is likely some tilt in the H&E image *versus* the SECM image due to the embedding and sectioning process.

3.3 *FFOCM*

Figure 3(a)–3(c) shows images obtained from a rat lung slice with FFOCM from all three spatial planes, with H&E histology from the same sample in Fig. 3(d). The alveolar walls can be clearly delineated and the capillary network inside the walls was visible as non-scattering media surrounded by the scattering endothelium (arrows). Cells that are likely to be type II alveolar pneumocytes (stars) are characterized as highly scattering with a relatively large size and shape compared to what would be expected for type I pneumocytes. However, individual type I pneumocytes could not be clearly identified. Blood vessels (V) were identified and their endothelium was distinguished from the blood content due to high scattering from the nuclei of the endothelial cells. Blood cells could also be visualized with a crenated appearance, likely due to the fixation process. The maximum imaging depth reached beyond 250 μm when imaging through the PBS-immersed airspaces, but the strong blood attenuation limited the imaging depth to less than 50 μm when imaging through blood filled vessels. Thirty randomly chosen alveolar walls were measured with a FWHM thickness of 4.8 ± 3.3 μm (mean $\pm$ standard deviation).

3.4 *Comparison of Imaging Techniques*

Figure 4 compares images from all three reflectance imaging techniques of a fixed PBS-immersed rat lung slice acquired within the same field of view. Figure 4(a)–4(c) shows *en-face* OFDI and SECM sections with the corresponding histology; and Fig. 4(d)–4(f) shows zoomed-in regions of the OFDI and SECM images that correspond to the FFOCM field of view. These images illustrate the difference in resolution and expected image quality between the techniques. Table 2 summarizes the performance of OFDI, SECM, and FFOCM for imaging PBS-immersed, fixed rat lung tissue slices, as described below.

OFDI provided high frame rates and the largest imaging depth for the specific systems used in this study. The lower

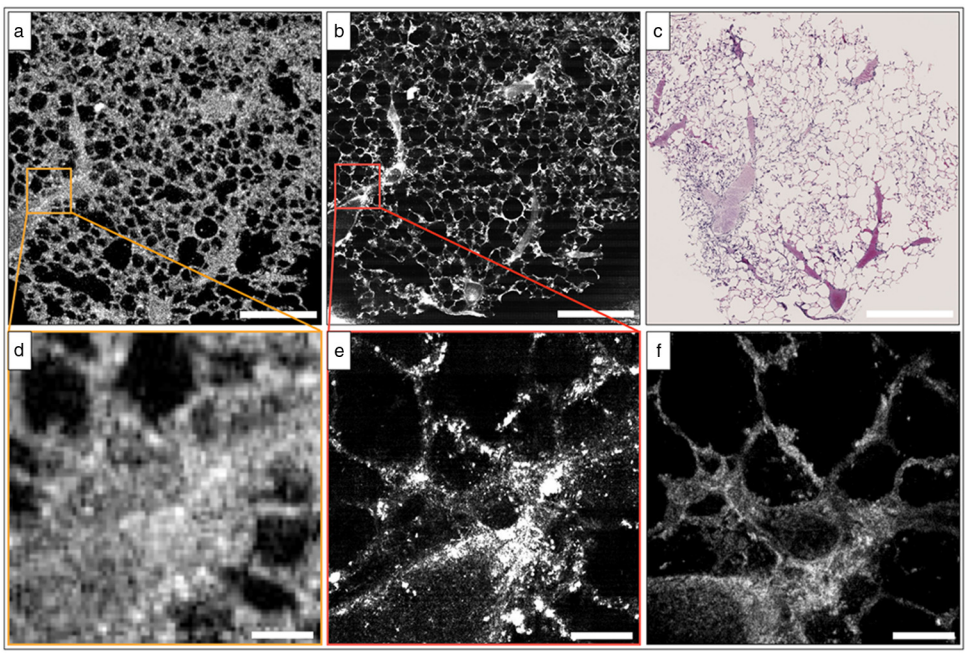

Fig. 4 OFDI, SECM, FFOCM and H&E histology images of PBS immersed fixed rat lung slice. (a) OFDI, (b) SECM, and (c) H&E histology within the *en-face* plane, where scale bar = 500 μm. (d) OFDI and (e) SECM images in greater detail matched with (f) FFOCM image, where scale bar = 50 μm.

Table 2 Summary of performance criteria for current OFDI, SECM, and FFOCM systems to image PBS-immersed rat lung tissue.

Performance criteria	OFDI	SECM	FFOCM
Structures observed	Alveolar walls Blood vessels	Alveolar walls Blood vessels Type II pneumocytes	Alveolar walls Blood vessels, Type II pneumocytes Capillaries, Crenated erythrocytes
Primary advantage	Imaging speed Imaging depth	High transverse resolution Potential for high imaging speed	High isotropic resolution
Primary disadvantage	Lower resolution	Imaging depth	Imaging speed
Imaging probes	Miniaturized catheter (0.8 mm) and needle probes	Hand-held probes at 10 mm diameter	Currently no miniaturized probe

transverse resolution of the system resulted in images with thicker alveolar walls, but the majority of the airspaces and vessels were still visualized within the rat lung samples. OFDI might therefore provide the most practical option for evaluating alveoli over a relatively large tissue volume. The high acquisition speed may also enable alveolar imaging where motion artifacts hinder current technologies such as micro-CT.

OCT imaging has already been performed during bronchoscopy and visualized intact alveolar attachments to the small airways.[26] As catheters become smaller, more regions surrounding thin walled airways could be reached in a minimally invasive way that limits any changes to the alveolar environment. Currently, 0.8 mm diameter optical catheters are used in the clinical setting to assess coronary arteries.[27] It is important to note that bronchoscopic access limits the analysis to alveolar features immediately surrounding the airways.

Subpleural alveoli could be evaluated in an open-chest procedure or through an optical window as previously demonstrated in a rabbit model by Meissner et al.[6] In addition to requiring mechanical ventilation, this route of access currently removes any local effect the chest wall has on the alveolar environment. Lastly, OCT-based needle probes have also been demonstrated[19,28,29] to provide access to lung parenchyma that cannot be visualized through the airways or the pleura with optical imaging techniques. However, this route of access comes at the cost of local trauma to the tissue and the possibility of pneumothorax as well as drag artifacts caused by needle movement.

SECM provided much higher resolutions in the lateral (1.3 μm), and axial direction (2.4 μm) than OFDI and could visualize type II pneumocytes. The high resolution of SECM could also provide absolute measurements of alveolar wall thickness and identification of inflammatory cells. The usable imaging depth with the current system configuration was 100 to 150 μm, which was the lowest of the three techniques. The potential of SECM for imaging at high speeds may facilitate the acquisition of large fields of view and dynamic imaging, but miniature probes are not currently available. Forward-scanning and helical-scanning probes have been demonstrated at diameters of 10 mm[23,30,31] with the promise to further reduce the probe diameter up to 5 mm.[31] At this development stage, only imaging through a pleural window or an open chest procedure seems possible.[32] To enable endoscopic imaging, probe diameters $\leq$1 mm would be most practical, allowing the probe to be inserted into the working channel of any adult bronchoscope and reach later generations with thinner airway walls. Confocal fluorescence microscopy has been demonstrated for *in vivo* alveolar imaging through a bronchoscope and via penetration through the distal bronchiolar wall.[33] A confocal imaging probe to be inserted in a 22 gauge needle has recently been developed for biological tissue.[34]

FFOCM provided the best spatial resolution of all three techniques and would be best suited to evaluate absolute alveolar wall thickness in different species and pathophysiologic changes such as wall thickening or inflammatory cell recruitment. The 1-μm isotropic resolution of FFOCM provides the ability to analyze 3-D structures down to a few micrometers, which could potentially be useful for identifying and characterizing individual cells such as alveolar type I or II, macrophages or eosinophils. FFOCM currently provides the slowest acquisition speed of the three imaging systems, however, and the development of miniaturized probes for both *in vivo* and *ex-vivo* imaging is still at an early stage. A FFOCM system with 1.5 million A-lines/s acquisition has been demonstrated with a spatial resolution around 13 μm.[35] A miniaturized 2 mm diameter probe has also been demonstrated with a resolution of 3.5 and 1.8 μm in the lateral and axial direction, respectively.[36]

3.5 *Study Limitations*

This study investigated the use of three reflectance optical imaging techniques to image lung tissue from a single species, the rat. However, we expect our conclusions to translate to all mammalian species, including the ability to visualize cells (where applicable), airspaces, blood vessels, and alveolar walls within the specified imaging depths. The structures of the alveolar regions of the lung are conserved across all mammalian species, with only a change in alveolar size and alveolar interstitial thickness.[37]

In this paper, we investigated the advantages and limitations of the different technologies with respect to resolution, field of view, and imaging depth. These parameters are in part specific to the current device configurations. For example, the OFDI configuration implemented within this study could not resolve alveoli less than 20 to 30 μm in diameter, which could be limiting in a mouse model. However, this limitation is not intrinsic to the technology as high-transverse resolution OFDI can be performed with a higher NA lens. It is reasonable to expect improved cellular detail within a decreased imaging depth by

implementing a larger NA lens within the OFDI sample arm probe. SECM, as implemented here, obtained images using a swept-source laser with a 5 kHz line rate, resulting in several minute acquisition times. Newer lasers with rates up to and exceeding 1 MHz have been developed, and it is likely the combination with high speed detection systems would allow imaging at image acquisition speeds that are 1 to 2 orders of magnitude greater than video rate. It is also important to note that the field of view of the current FFOCM system might present difficulties when attempting to image multiple alveoli within larger species. Again, this limitation is specific to the imaging system we used in the study and not intrinsic to the technique itself.

All samples were filled with PBS and not air, as would be the case in a normal respiring lung. Although some alveoli could in principle be fluid filled during various clinical conditions, such as bronchoalveolar lavage, liquid breathing, or edema, additional challenges will arise when translating these technologies for imaging air-filled alveoli *in vivo*. It is important to note that significant differences in image quality are expected for fluid-*versus* air-filled alveoli as light refracts substantially when encountering high refractive index differences between tissue and air. We therefore expect the imaging depth of the tested technologies to be greatly reduced when the alveoli are filled with air, as previously demonstrated in ethanol-filled rabbit lungs using spectral-domain OCT,[38] that resulted in distorted alveolar shapes.

This study was conducted in fixed lung tissue for practical reasons. In doing so, the same field of view could be imaged with all three technologies at the same inflation state. Furthermore, the lung could be cut into slices, which allowed the evaluation of any location within the lung compared to limiting the analysis to the alveolar layers directly beneath the pleura. The difference in refractive index between fresh and fixed tissue impacts both the resolution and imaging depth. Fixed tissue has a higher refractive index due to the polyethylene glycol (1.47 at 20ºC) and we expect PBS-immersed fresh lungs will show decreased refraction artifacts and slightly increased imaging depth at the cost of a decrease in contrast and/or resolution. In addition, light scattering by unfixed blood will decrease the imaging depth depending on the size of the vessel within the field of view.[39]

We have presented a limited number of direct correlations to histology, which does not allow verification of all structures visible in the images. Due to the additional processing cycles between image acquisition and H&E sectioning, the fine structures of the alveolar walls are distorted and difficult to recognize. Often intact histology sections could only be obtained after cutting up to 100 μm from the tissue surface. Correlative histology was also difficult to find due to the limited imaging depth of the technologies. While these difficulties limited our ability to analyze the data, they emphasized the importance of imaging techniques that provide non-destructive assessment of alveolar structure and function.

4 Conclusion

In this paper, we demonstrated that three reflectance microscopy imaging technologies could visualize the small airways, individual alveoli and blood vessels in fixed, PBS-immersed rat lung slices without administration of contrast agents or radiation exposure. Our findings suggest that FFOCM provides the best results for applications requiring absolute measurements of alveolar wall thickness or identification of specific cell-types. SECM, with similar resolution and higher speed, is likely better suited for cellular resolution imaging over larger fields of view. OFDI has reduced resolution compared with FFOCM and SECM but is still adequate for the observation of relative alveolar sizes or a gross identification of airspaces and vessels. In addition, OFDI provides high-speed evaluation over very large fields of view and is currently the most promising to be incorporated into an *in vivo* imaging probe.

Compared to histology, the most commonly used method for visualizing alveolar structures, the reflectance imaging methods are non-destructive and do not require embedding, sectioning or staining, which are known to create shrinkage, compression and tearing artifacts.[1] Further, no tissue is lost during optical sectioning and the 3-D dataset can be virtually sliced and analyzed at oblique angles. Micro-CT does provide comparable resolution to the optical techniques with much greater penetration depth. The acquisition time is dependent on the resolution and sample size, but is much longer than OFDI and comparable to SECM for the same resolution and size. However, because the resolution of micro-CT decreases with sample size, it cannot currently be translated to whole lung alveolar imaging in species larger than rats. While optical technologies can only obtain images with a penetration depth of a few hundred micrometers, high-resolution images can be acquired from large samples, making these techniques amenable to studying subsurface alveoli in large animals and humans.

Acknowledgments

The authors thank Jenny Zhao and the Wellman Center Photopathology Laboratory staff for expert histology processing, and Joseph Gardecki and Yukako Yagi for their help digitizing the histology. This work was supported by Air Liquide, Medical Gases, Les-Loges-en-Josas, France.

References

1. C. C. Hsia et al., "An official research policy statement of the American Thoracic Society/European Respiratory Society: standards for quantitative assessment of lung structure," *Am. J. Respir. Crit. Care Med.* **181**(4), 394–418 (2010).
2. R. R. Mercer, J. M. Laco, and J. D. Crapo, "Three-dimensional reconstruction of alveoli in the rat lung for pressure-volume relationships," *J. Appl. Physiol.* **62**(4), 1480–1487 (1987).
3. H. D. Litzlbauer et al., "Three-dimensional imaging and morphometric analysis of alveolar tissue from microfocal X-ray-computed tomography," *Am. J. Physiol. Lung Cell Mol. Physiol.* **291**(3), L535–545 (2006).
4. S. Dhondt et al., "Plant structure visualization by high-resolution X-ray computed tomography," *Trends Plant Sci.* **15**(8), 419–422 (2010).
5. E. L. Ritman, "Micro-computed tomography of the lungs and pulmonary-vascular system," *Proc. Am. Thorac. Soc.* **2**(6), 477–480 (2005).
6. S. Meissner et al., "Three-dimensional Fourier domain optical coherence tomography in vivo imaging of alveolar tissue in the intact thorax using the parietal pleura as a window," *J. Biomed. Opt.* **15**(1), 016030 (2010).
7. E. Namati et al., "Alveolar dynamics during respiration: are the pores of Kohn a pathway to recruitment?," *Am. J. Respir. Cell Mol. Biol.* **38**(5), 572–578 (2008).
8. S. Yun et al., "High-speed optical frequency-domain imaging," *Opt. Express* **11**(22), 2953–2963 (2003).
9. M. Choma et al., "Sensitivity advantage of swept source and Fourier domain optical coherence tomography," *Opt. Express* **11**(18), 2183–2189 (2003).

10. C. Boudoux et al., "Rapid wavelength-swept spectrally encoded confocal microscopy," *Opt. Express* **13**(20), 8214–8221 (2005).
11. E. Beaurepaire et al., "Full-field optical coherence microscopy," *Opt. Lett.* **23**(4), 244–246 (1998).
12. D. O. Slauson and F. F. Hahn, "Criteria for development of animal models of diseases of the respiratory system: the comparative approach in respiratory disease model development," *Am. J. Pathol.* **101**(3 Suppl), S103–122 (1980).
13. K. R. Stenmark et al., "Animal models of pulmonary arterial hypertension: the hope for etiological discovery and pharmacological cure," *Am. J. Physiol. Lung Cell Mol. Physiol.* **297**(6), L1013–1032 (2009).
14. G. R. Zosky and P. D. Sly, "Animal models of asthma," *Clin. Exp. Allergy* **37**(7), 973–988 (2007).
15. J. L. Wright, M. Cosio, and A. Churg, "Animal models of chronic obstructive pulmonary disease," *Am. J. Physiol. Lung Cell Mol. Physiol.* **295**(1), L1–15 (2008).
16. E. Namati et al., "Large image microscope array for the compilation of multimodality whole organ image databases," *Anat. Rec. (Hoboken)* **290**(11), 1377–1387 (2007).
17. J. G. Fujimoto et al., "Optical biopsy and imaging using optical coherence tomography," *Nat. Med.* **1**(9), 970–972 (1995).
18. R. Leitgeb, C. Hitzenberger, and A. Fercher, "Performance of fourier domain vs. time domain optical coherence tomography," *Opt. Express* **11**(8), 889–894 (2003).
19. G. J. Tearney et al., "In vivo endoscopic optical biopsy with optical coherence tomography," *Science* **276**(5321), 2037–2039 (1997).
20. D. Huang et al., "Optical coherence tomography," *Science* **254**(5035), 1178–1181 (1991).
21. S. H. Yun et al., "Comprehensive volumetric optical microscopy in vivo," *Nat. Med.* **12**(12), 1429–1433 (2006).
22. G. J. Tearney, R. H. Webb, and B. E. Bouma, "Spectrally encoded confocal microscopy," *Opt. Lett.* **23**(15), 1152–1154 (1998).
23. D. Kang et al., "Comprehensive volumetric confocal microscopy with adaptive focusing," *Biomed. Opt. Express* **2**(6), 1412–1422 (2011).
24. Y. K. Tao and J. A. Izatt, "Spectrally encoded confocal scanning laser ophthalmoscopy," *Opt. Lett.* **35**(4), 574–576 (2010).
25. W. Y. Oh et al., "ltrahigh-resolution full-field optical coherence microscopy using InGaAs camera,"*Opt. Express* **14**(2), 726–735 (2006).
26. H. O. Coxson et al., "New and current clinical imaging techniques to study chronic obstructive pulmonary disease," *Am. J. Respir. Crit. Care Med.* **180**(7), 588–597 (2009).
27. G. J. Tearney and B. E. Bouma, "Shedding light on bioabsorbable stent struts seen by optical coherence tomography in the ABSORB trial," *Circulation* **122**(22), 2234–2235 (2010).
28. R. A. McLaughlin and D. D. Sampson, "Clinical applications of fiber-optic probes in optical coherence tomography," *Opt. Fiber Technol.* **16**(6) 467–475 (2010).
29. B. C. Quirk et al., "In situ imaging of lung alveoli with an optical coherence tomography needle probe," *J. Biomed. Opt.* **16**(3), 036009 (2011).
30. C. Boudoux et al., "Optical microscopy of the pediatric vocal fold," *Arch. Otolaryngol. Head Neck Surg.* **135**(1), 53–64 (2009).
31. C. Pitris et al., "A GRISM-based probe for spectrally encoded confocal microscopy," *Opt. Express* **11**(2), 120–124 (2003).
32. M. Czaplik et al., "Methods for quantitative evaluation of alveolar structure during in vivo microscopy," *Respir. Physiol. Neurobiol.* **176**(3), 123–129 (2011).
33. L. Thiberville et al., "Confocal fluorescence endomicroscopy of the human airways," *Proc. Am. Thorac. Soc.* **6**(5), 444–449 (2009).
34. R. S. Pillai, D. Lorenser, and D. D. Sampson, "Deep-tissue access with confocal fluorescence microendoscopy through hypodermic needles," *Opt. Express* **19**(8), 7213–7221 (2011).
35. T. Bonin et al., "In vivo Fourier-domain full-field OCT of the human retina with 1.5 million A−lines/s," *Opt. Lett.* **35**(20), 3432–3434 (2010).
36. A. Latrive and A. C. Boccara, "In vivo and in situ cellular imaging full-field optical coherence tomography with a rigid endoscopic probe," *Biomed. Opt. Express* **2**(**10**), 2897–2904 (2011).
37. R. R. Mercer, M. L. Russell, and J. D. Crapo, "Alveolar septal structure in different species," *J. Appl. Physiol.* **77**(3), 1060–1066 (1994).
38. S. Meissner, L. Knels, and E. Koch, "Improved three-dimensional Fourier domain optical coherence tomography by index matching in alveolar structures," *J. Biomed. Opt.* **14**(6), 064037 (2009).
39. M. Brezinski et al., "Index matching to improve optical coherence tomography imaging through blood," *Circulation* **103**(15) (2001).